

Background-free collinear autocorrelation and frequency-resolved optical gating using mode multiplexing and demultiplexing in aperiodically poled lithium niobate waveguides

Carsten Langrock* and M. M. Fejer

Edward L. Ginzton Laboratory, Stanford University, Stanford, California 94305-4085, USA

*Corresponding author: langrock@stanford.edu

Received March 28, 2007; revised May 23, 2007; accepted June 12, 2007;
posted June 28, 2007 (Doc. ID 81566); published August 2, 2007

We use mode multiplexing and demultiplexing in apodized aperiodically poled lithium niobate waveguides to enable characterization of picosecond optical pulses in a collinear but background-free way using autocorrelation and second-harmonic frequency-resolved optical gating. © 2007 Optical Society of America
OCIS codes: 190.1900, 190.4390.

In this Letter, we present a new device for implementation of second-harmonic generation (SHG) autocorrelation and frequency-resolved optical gating [1] (SHG-FROG) of ultrafast optical pulses. Conventional SHG autocorrelation and SHG-FROG can be implemented in either collinear or noncollinear geometries. The collinear geometry can be further divided into copolarized and perpendicularly polarized implementations. In general, using a noncollinear, and therefore noninterferometric, geometry dictates the use of a relatively inefficient bulk nonlinear element, while allowing easy spatial discrimination between the autocorrelation SH signal and the SH produced by each pulse separately. The collinear geometry can take advantage of highly efficient guided-wave nonlinear materials, while exhibiting interferometric effects when copolarized beams are used. In this geometry, each pulse itself will produce SH collinear with the autocorrelation SH signal, resulting in a nonzero background. The devices described in this Letter combine three features: a waveguide geometry to increase the efficiency compared with bulk devices, a linearly chirped quasi-phase-matched (QPM) grating to increase the bandwidth of the SHG process, and two-mode operation with integrated multiplexers and demultiplexers to enable background-free operation.

The nonlinear elements used here are reverse-proton-exchanged (RPE) apodized aperiodically poled lithium niobate (apodized A-PPLN) waveguides [2,3]. By aperiodic, we mean a change in local periodicity of the QPM grating as a function of position along the propagation direction z . Following the nomenclature introduced in [4], we can assign a grating k vector $K_g(z)$ to the local QPM period $K_g(z) = 2\pi/\Lambda(z)$. We call a QPM grating linearly chirped, if $K_g(z)$ varies linearly along z , $K_g(z) = K_m + 2D_g z$. Here, $K_m = \Delta k_0 = 2k_{\text{FH}} - k_{\text{SH}}$ is set by the usual phase-matching condition for SHG at a convenient reference frequency (typically at one end of the spectrum of the pulse to be characterized), and $D_g = \text{const}$ is the grating chirp parameter. While the conversion bandwidth of a periodic (i.e., uniform) QPM grating is inversely propor-

tional to the length of the grating [e.g., 0.25-nm full width at half-maximum (FWHM) for a 5-cm-long grating, see Fig. 1(a)], the bandwidth of a linearly chirped grating can be engineered by properly choosing D_g . One should note that the peak conversion efficiency of a given linearly chirped QPM grating is inversely proportional to its conversion bandwidth; e.g., a 5-cm-long 50-nm-wide QPM grating will have a peak conversion efficiency that is 200 times lower than that of a uniform grating of equal length [see Fig. 1(b)]. While not taken advantage of in this work, it is also possible to engineer the phase of the transfer function with chirped gratings, for example, to shape SH pulses [5].

For the case of SHG, there exists an analytical expression for a QPM grating's transfer function given $K_g(z)$ [4]. The transfer function and the grating k vector form a Fourier transform pair. This explains the pronounced ripple present in the SHG transfer function shown in Fig. 1(b); the abrupt beginning and end of the QPM grating results in high spatial frequen-

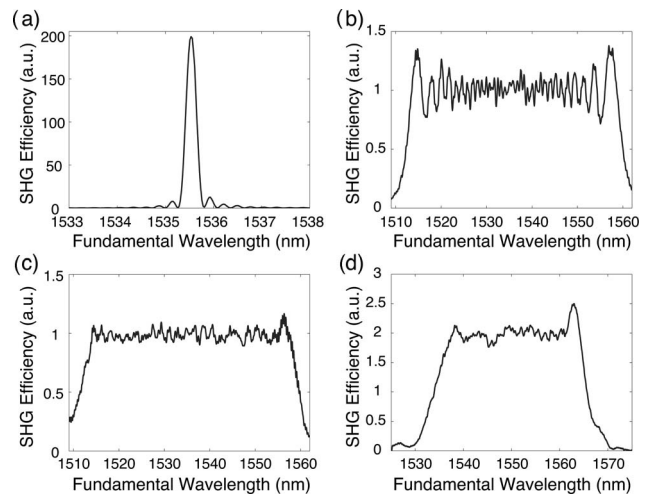


Fig. 1. Experimental SHG transfer functions of a (a) uniform, (b) 50-nm-wide chirped, (c) 50-nm-wide chirped and apodized, and (d) 25-nm-wide chirped and apodized QPM grating. Note that the product of efficiency and bandwidth is approximately the same for all cases.

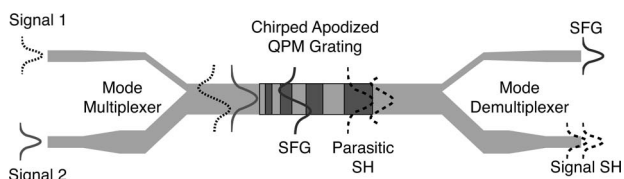


Fig. 2. Schematic of an asymmetric Y-junction device showing mode multiplexer at the input and demultiplexer at the output. Note that an odd SH spatial mode can be generated only through mixing an even and an odd FH mode, and so contains only SFG and not SH contributions.

cies in the transform domain and therefore in ripples in the transfer function. Because these ripples are rarely desirable, methods have been developed to reduce them. The underlying principle of these methods is the control of the local nonlinearity. A slow increase and decrease of the local nonlinearity at the beginning and end of the QPM grating, respectively, eliminate the high spatial frequencies of hard-edged gratings. Some of the methods to achieve this apodization of the local nonlinearity in guided-wave QPM structures are described in detail in [2]. When applied to linearly chirped QPM gratings, they can significantly reduce the amount of ripple within the conversion bandwidth as shown in Figs. 1(c) and 1(d). We used the deleted-reversal apodization technique for the devices used in this experiment.

It has been demonstrated that these apodized A-PPLN RPE waveguides provide excellent sensitivity and bandwidth for the characterization of femtosecond optical pulses [3,6,7], with autocorrelation results demonstrated at energies as low as 52 aJ [6] and SHG-FROG results at 124 aJ [3]. Since protonated waveguides support only a single polarization (TM), the collinear copolarized SHG geometry will cause background SH and interferometric effects. Using on-chip mode multiplexing and demultiplexing in two-mode RPE PPLN waveguides [8] as shown in Fig. 2, we are able to greatly reduce the interferometric oscillations and almost completely remove the background. The efficiency of the devices described here is within a factor of approximately two of the simpler straight-waveguide devices.

These devices are based on the launching and separation of higher-order waveguide modes with high contrast using asymmetric Y junctions. As depicted in Fig. 2, one of the inputs (signal 1) is launched into the TM_{10} mode, while the other input (signal 2) is launched into the waveguide's lowest-order mode, TM_{00} . The sum-frequency product (SFG) between these two spatial modes is generated in the TM_{10} mode (resembling a type II phase-matched interaction), while the SH of each input appears in an even-order mode, TM_{20} and TM_{00} , respectively. The sum frequency can then be separated from each pulse's SH component by the output asymmetric Y junction, resulting in a collinear but background-free interaction. The resulting autocorrelation traces and SHG-FROG data are ideally the same as the ones obtained with conventional background-free methods, while taking advantage of the large nonlinear conversion efficiency available in engineered QPM waveguide structures.

We implemented two different experimental setups to compare single-mode waveguides to mode-multiplexed ones (Fig. 3). In either setup we used light from a mode-locked Ti:sapphire-synchronously-pumped optical parametric oscillator (OPO) (Spectra-Physics Tsunami & Opal) at 1550 nm as the input to our experiment. This light was coupled into an SMF-28 fiber via a fiber-coupled collimator before being bandpass filtered using a thin-film filter (1 nm FWHM). The pulses were split into two identical copies using a 3 dB coupler. One replica was sent through a fixed delay, while the other passed through a variable delay line (General Photonics MDL-001). In the conventional setup [A, Fig. 3(a)], the delayed copies were then recombined in a second 3 dB splitter before being coupled into a fiber-pigtailed A-PPLN waveguide whose transfer function is shown in Fig. 1(d). The setup using the mode-multiplexing structure [B, Fig. 3(b)] did not require the second 3 dB splitter due to the on-chip mode multiplexing (see Fig. 2). Here, two single-mode fibers were directly pigtailed to the inputs of the A-PPLN device [transfer function similar to Fig. 1(d)]. The power and spectral content of the generated SHG as a function of relative temporal delay were recorded using a silicon detector and fiber-coupled handheld spectrometer (Ocean Optics HR4000), respectively.

Unlike conventional type II SHG-FROG in a uniform crystal [9], the association in a chirped crystal of each generated wavelength with a specific location (and hence group-velocity mismatch-induced time delay) allows straightforward removal of the spectral shear. In this case, the limit on the shortest usable pulse length arises from group-velocity dispersion (GVD), as in type I SHG-FROG. Given the GVD parameter β_2 and device length L , the shortest supported pulse length of a transform-limited Gaussian pulse is $\tau_{\min} \approx \sqrt{\beta_2 L / \sqrt{(1+\epsilon)^2 - 1}}$, accepting a fractional pulse broadening of ϵ over the length of the device. With the device parameters $\beta_2 \approx 100 \text{ fs}^2/\text{mm}$ at

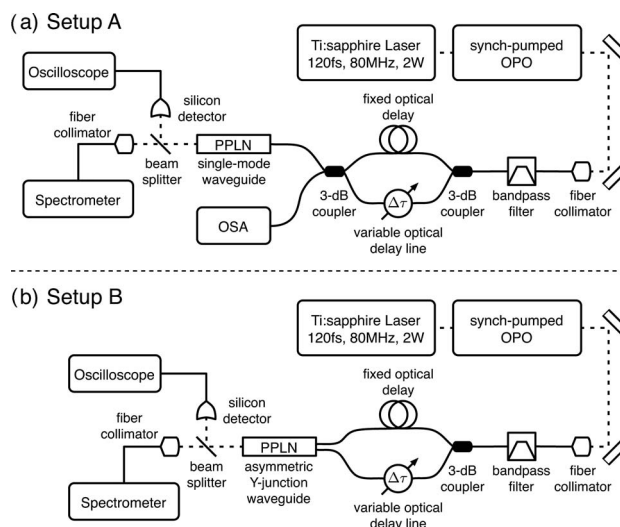


Fig. 3. Schematic of experimental setup used for autocorrelation and FROG measurements. (a) Setup A contains a single-mode A-PPLN waveguide, while (b) setup B contains a mode-multiplexing waveguide structure. OSA, optical spectrum analyzer. Other terms defined in text.

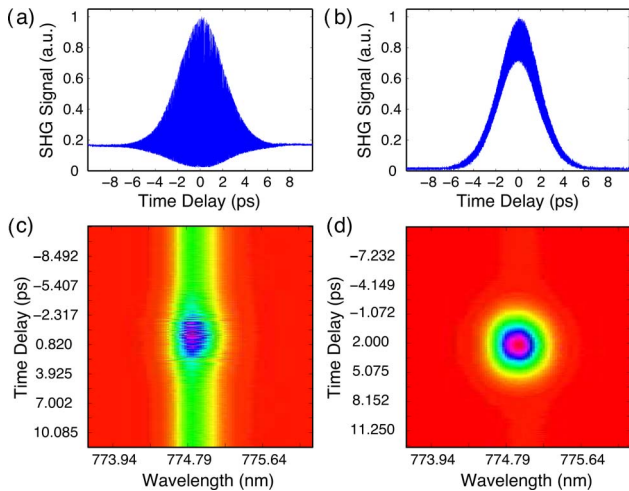


Fig. 4. (Color online) (a) Autocorrelation trace and (b) FROG data and plot of integrated spectral power obtained using interferometric setup A.

1550 nm, $L=5$ cm, and $\epsilon=1\%$, $\tau_{\min} \approx 190$ fs. We will discuss these limitations in more detail in future work.

Proper operation of our setups was confirmed by measuring the autocorrelation function of the input pulses. The interferometric autocorrelation trace obtained with setup A is shown in Fig. 4(a). By assuming a Gaussian pulse envelope, the FWHM pulse duration τ_p is calculated to be 3.09 ps ($\tau_p/\tau_{ac}=0.6523$, with τ_{ac} being the autocorrelation's FWHM), while the shape of the interferometric autocorrelation trace indicates the absence of frequency chirp. Repeating this measurement with the background-free setup B, we obtained $\tau_p=3.04$ ps ($\tau_p/\tau_{ac}=1/\sqrt{2}$). Note that while the wings of the intensity autocorrelation trace shown in Fig. 4(b) approach zero, the finite modal contrast of 23 dB within the device causes residual interference fringes. Improved mode multiplexers at the input of the device should allow for a further reduction of these fringes. Mode multiplexers with contrast ratios approaching 30 dB have been demonstrated [8]. These fringes do not pose a problem for FROG measurements as long as the spectrometer's integration time is long enough with respect to the rate of delay change to average them out. To obtain the results shown in Figs. 4(a) and Fig. 4(b), the delay line was swept with 1 ps/s across a 20 ps delay range.

Replacing the silicon detector with the spectrometer, we recorded the SH spectra as a function of delay position across a 40 ps delay range, sweeping the delay with 0.25 ps/s. The spectrometer was set to integrate for 10 ms and average over 5 consecutive traces. The spectrometer's resolution in the region of interest was 0.025 nm, allowing for sufficiently resolved spectra. The FROG trace shown in Fig. 4(c) was obtained using setup A, while the one shown in Fig. 4(d) was taken with setup B. The elimination of the background contribution using setup B reduced the overall offset of the data, while the significant re-

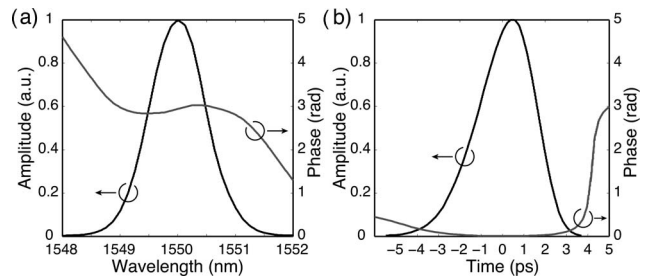


Fig. 5. Calculated (a) spectral and (b) temporal amplitude and phase information using a FROG retrieval algorithm.

duction in interference resulted in a much improved smoothness.

The background-free FROG trace [Fig. 4(d)] was input into a SHG-FROG retrieval algorithm (FemtoSoft FROG) to recover amplitude and phase information. The retrieved spectrum and temporal profile are shown in Fig. 5. The spectral FWHM was calculated to be 1.13 nm, while the temporal FWHM was 3.17 ps. The FROG error in this calculation was below 0.0009.

In conclusion, we demonstrated that mode multiplexing and demultiplexing in apodized A-PPLN RPE waveguides can facilitate collinear but background-free autocorrelation and SHG-FROG of ultrashort optical pulses. The usefulness of these device structures is not limited to the above mentioned techniques, but will support other characterization schemes such as X-FROG and SPIDER as well.

We thank A. M. Weiner for useful discussions of GVM-induced limitations in type II autocorrelation measurements. This research was sponsored by the Air Force Office of Scientific Research (AFOSR grant FA9550-05-1-0180), the National Science Foundation through Purdue University (NSF Prime ECS-0401515), the Department of Energy through Lawrence Livermore National Laboratory (DOE Prime W-7405-ENG-48), and Crystal Technology, Inc.

References

1. D. J. Kane and R. Trebino, *IEEE J. Quantum Electron.* **29**, 571 (1993).
2. J. Huang, X. P. Xie, C. Langrock, R. V. Roussev, D. S. Hum, and M. M. Fejer, *Opt. Lett.* **31**, 604 (2006).
3. S.-D. Yang, A. M. Weiner, K. R. Parameswaran, and M. M. Fejer, *Opt. Lett.* **30**, 2164 (2005).
4. G. Imeshev, M. A. Arbore, M. M. Fejer, A. Galvanauskas, M. Fermann, and D. Harter, *J. Opt. Soc. Am. B* **17**, 304 (2000).
5. A. M. Schober, G. Imeshev, and M. M. Fejer, *Opt. Lett.* **27**, 1129 (2002).
6. S.-D. Yang, A. M. Weiner, K. R. Parameswaran, and M. M. Fejer, *Opt. Lett.* **29**, 2070 (2004).
7. J. Prawiharjo, K. Gallo, B. C. Thomsen, M. A. F. Roelens, P. J. Almeida, N. G. R. Broderick, and D. J. Richardson, *IEEE Photon. Technol. Lett.* **17**, 849 (2005).
8. J. R. Kurz, J. Huang, X. Xie, T. Saida, and M. M. Fejer, *Opt. Lett.* **29**, 551 (2004).
9. A. M. Weiner, *IEEE J. Quantum Electron.* **19**, 1276 (1983).